RSC Advances

PAPER

View Article Online
View Journal | View Issue

Cite this: *RSC Adv.*, 2026, **16**, 23280

Etching-induced morphological evolution of concave gold nanocubes for enhanced colorimetric sensing of cobalt ions based on Fenton-like reactions

Yi Yu,[a] Qin Zou,[bc] Xinghua Xiang,[a] Zhang Chen[bc] and Ling Lin *[bcd]

Cobalt is an essential trace element for human growth and development, but both its deficiency and excess can cause adverse health effects. Herein, we develop a rapid, visual, and highly sensitive colorimetric sensor for Co^{2+} detection using concave gold nanocubes (CGNs) as a novel probe based on a Fenton-like reaction-mediated etching mechanism. In the presence of H_2O_2 and Co^{2+}, a Fenton-like reaction occurs and generates abundant superoxide radicals, which oxidize Au^0 on CGNs surface to generate $Au(SCN)_2^-$, leading to a morphological transformation from concave to spherical shapes. This process causes a significant reduction in the absorbance at 690 nm in the UV-vis spectrum of the sensor, while the absorbance at 535 nm increases apparently. Under optimized conditions (2.0 mM KSCN, pH 9.0, and a reaction time of 18 min), the sensor exhibits a good linear relationship between the absorbance ratio (A_{535}/A_{690}) and Co^{2+} concentration over the range of 0.5–400 nM, with a linear regression equation of $A_{535}/A_{690} = 0.00798C_{Co^{2+}} + 0.6128$ and $R^2 = 0.9906$. Its limit of detection is 0.3 nM, surpassing that of most reported sensors, because of the high chemical activity and morphology-dependent optical properties of CGNs. This sensor shows excellent selectivity against common interfering ions (*e.g.*, Mn^{2+} and Hg^{2+}) and detects Co^{2+} in real water samples with good recoveries. This study proves that CGNs are efficient probes for the development of sensitive assays, which hold great potential in food safety and environmental monitoring applications.

Received 11th January 2026
Accepted 25th March 2026

DOI: 10.1039/d6ra00268d

rsc.li/rsc-advances

1. Introduction

As a vital trace element, cobalt is the critical component of vitamin B_{12} and plays an important role in hemoglobin synthesis and hematopoiesis.[1,2] The total amount of cobalt in the human body is around 3 mg, and its daily intake by humans from diet is 10–80 μg; its deficiency can cause many health problems such as pernicious anemia, growth retardation, and cardiovascular diseases.[3,4] Nevertheless, its excessive exposure, probably through dietary intake, occupational contact, medical settings, and environmental pollution, poses serious threats to humans, including cardiomyopathy, allergic dermatitis, and enzyme activity inhibition.[5–7] On the another hand, industrial activities such as mining, hard metal production, and cement manufacturing are sources of cobalt contamination, leading to elevated cobalt levels in water, soil, and food.[6] Therefore, the development of rapid, sensitive, and low-cost assays for Co^{2+} detection is important not only for public health safety but also for environmental protection. The widely applied conventional methods for its detection include atomic absorption spectroscopy (AAS),[8] inductively coupled plasma atomic emission spectroscopy (ICP-AES),[9] potentiometric titration,[10] and fluorescence spectroscopy.[11] While these methods have good practical value, they still suffer from many inherent limitations such as time-consuming sample processing, complex instrumental operation, and reliance on expensive instrumentation, which restrict their on-site and routine applications.

Colorimetric sensors using gold nanomaterials possess many advantages including simplicity, rapid response, and visual readout capability, attributed to their specific localized surface plasmon resonance (LSPR) properties.[12–14] Their LSPR is determined by their sizes, shapes, and surface states.[15] Especially, concave gold nanocubes (CGNs), with six concave surfaces and eight sharp tips, stand out due to their high specific surface area, enhanced surface activity, and tunable LSPR properties.[16,17] Similar to gold nanostars, CGNs have abundant active sites for chemical reactions, making them ideal

[a]*Department of Hepatopancreatobiliary and Hernia Surgery, The First Hospital of Hunan University of Chinese Medicine, Changsha, Hunan 410000, China*

[b]*Department of General Surgery, Xiangya Hospital, Central South University, Changsha, Hunan 410008, China. E-mail: 120562794@qq.com; Tel: +86-731-83929900*

[c]*National Clinical Research Center for Geriatric Disorders (Xiangya Hospital), Changsha, Hunan, 410008, China*

[d]*Department of General Surgery, Turpan People's Hospital (Turpan Branch of National Clinical Research Center for Geriatric Disorders), Turpan, Xinjiang 838000, China*

probes for assays.[17] Previous studies have demonstrated that gold nanoparticle-etching based colorimetric sensors have attracted more attention than aggregation-induced ones because of their strong anti-interference ability, outstanding limit of detection (LOD), and improved accuracy and sensitivity.[18,19] For example, based on Pb^{2+}-catalyzed etching of gold nanostars by 2-mercaptoethanol and sodium thiosulfate, a colorimetric assay for picomolar Pb^{2+} determination was proposed, with the advantages of multicolor changes and sensitivity comparable to inductively coupled plasma mass spectrometry (ICP-MS).[20] According to a similar mechanism, spherical gold nanoparticles[21] and gold nanorods[22] were also applied for Pb^{2+} detection at the nanomolar level. Based on Co^{2+}-triggered Fenton-like reactions generating reactive oxygen species that etch gold nanorods and lead to a variation in LSPR, Co^{2+} could be detected with an LOD of 1 nM and 40 nM by UV-vis spectroscopy and the naked eyes, respectively.[23] However, the use of CGNs for colorimetric sensing applications is relatively rare. An important possible reason is that their synthesis is complicated and time-consuming. The typical seed-mediated method for CGNs proposed by Mirkin required multiple chemicals and an incubation time of 12 h.[24]

In this work, we proposed a sensitive colorimetric sensor for Co^{2+} detection using CGNs as a probe based on Co^{2+} induced Fenton-like reactions. The recently reported simple preparation of CGNs in 10 min gives them great potential for application in analytical fields.[16,17] In the presence of H_2O_2, Co^{2+} induces the generation of abundant superoxide radicals ($O_2^{\bullet-}$) following a Fenton-like reaction, which oxidizes the Au^0 on the surface of CGNs to form $Au(SCN)_2^-$ in the presence of SCN^-, leading to the morphological transformation of CGNs from a concave to spherical shape. With an increase in the concentration of Co^{2+}, the solution color changes from blue to purple and red, accompanied by a reduction in absorbance at the longitudinal LSPR and an increase in absorbance at the transverse LSPR. Based on the specific catalytic reaction of Co^{2+}, this sensor exhibited high selectivity over other metal ions. Finally, the assay was validated for practical applicability in detecting real water samples with good performances. This study proves that CGNs are excellent probes for sensing due to their unique LSPR properties, which will find more applications in food and environmental sample detection.

2. Experimental

2.1 Chemicals

Hydrogen tetrachloroaurate ($HAuCl_4 \cdot 4H_2O$, ≥99.9%), cetyltrimethylammonium bromide (CTAB, ≥99%), sodium bicarbonate ($NaHCO_3$, ≥99%), potassium thiocyanate (KSCN, ≥99%), hydrogen peroxide (H_2O_2, 33%), ascorbic acid (AA, ≥99.5%), potassium chloride (KCl), calcium chloride ($CaCl_2$), sodium chloride (NaCl), magnesium chloride ($MgCl_2$), zinc chloride ($ZnCl_2$), mercuric nitrate ($HgNO_3$), stannous chloride dihydrate ($SnCl_2 \cdot 2H_2O$), cadmium chloride ($CdCl_2$), manganese sulphate ($MnSO_4$), copper sulfate pentahydrate ($CuSO_4 \cdot 5H_2O$), nickel chloride hexahydrate ($NiCl_2 \cdot 6H_2O$, ≥99%), iron(III) chloride hexahydrate ($FeCl_3 \cdot 6H_2O$, ≥99%) and cobalt sulfate heptahydrate ($CoSO_4 \cdot 7H_2O$, ≥99%) were purchased from Sinopharm Chemical Reagent Co., Ltd (Shanghai, China). All reagents were of analytical grade and used without further purification. Standard stock solutions of Co^{2+} (1 mM) were freshly prepared in ultrapure water and diluted to working concentrations immediately prior to use. Deionized water (18.2 MΩ cm) was obtained from a Millipore Milli-Q purification system and used throughout the experiments.

2.2 Apparatus

UV-vis absorption spectra were recorded using a UV-1800 spectrophotometer (Shimadzu, Kyoto, Japan). Transmission electron microscopy (TEM) images were obtained with a FEI Tecnai G220S-Twin microscope (FEI, Hillsboro, OR, USA) operating at 200 kV. pH was measured using a PHS-3C pH meter (Shanghai Yidian Scientific Instruments Co., Ltd, Shanghai, China). A H1650-W high-speed centrifuge (Hunan Xiangyi Laboratory Instrument Development Co., Ltd, Changsha, Hunan, China) and a DHG-9245A drying oven (Shanghai Baijiu Industry Co., Ltd, Shanghai, China) were used for sample preparation.

2.3 Synthesis of CGNs

CGNs were synthesized *via* a rapid seed-mediated growth method using AA and H_2O_2.[16,17] Briefly, 10 mL of CTAB solution (100 mM) was mixed with 206 μL of $HAuCl_4$ (24.28 mM), followed by the addition of 75 μL NaOH (1 M) to adjust the alkalinity and 10 μL of H_2O_2 (33%). The solution was vigorously stirred until it become transparent, indicating the transformation of Au^{3+} to Au^+, and then 300 μL of 100 mM AA was introduced to initialize the growth of CGNs. The reaction mixture was incubated at 30 °C for 10 min until its blue-greenish coloration remained unchanged, indicating the formation of CGNs with anisotropic facets. The resulting colloidal suspension was centrifuged at 8000 rpm for 15 min, washed three times with ultrapure water to remove excess surfactant, and finally redispersed in deionized water. The purified CGN suspension was stored at 4 °C for further use.

2.4 Sensitivity and selectivity for the detection of Co^{2+} using CGNs

For the colorimetric sensing experiments, 800 μL of a CGN dispersion was mixed with 30 μL CTAB (20 mM), 20 μL KSCN (100 mM), 25 μL $NaHCO_3$ (100 mM), and 40 μL H_2O_2 (33%) in the presence of varying concentrations of Co^{2+} solution. The total reaction volume was adjusted to 1.0 mL with deionized water. The mixture was incubated in a thermostatic water bath at 80 °C for 15 min to allow the Fenton-like reaction to etch CGNs. The resulting color changes were recorded using a mobile phone (Vivo S19, China) for visual analysis, and UV-vis absorption spectra were collected over the range of 400–1100 nm to quantitatively evaluate the variation in LSPR. The selectivity of the sensor was evaluated by testing common interfering ions, including Mn^{2+}, Hg^{2+}, Cu^{2+}, Ca^{2+}, Pb^{2+}, Cd^{2+}, Zn^{2+}, Sn^{2+}, Li^+, Na^+, Ni^{2+} and Fe^{3+}. The concentrations of these

interfering ions were kept at 1000 nM, which is 10-fold that of Co^{2+}.

2.5 Real sample analysis

Two water samples were collected from the Xiang River and a pond in Changsha, China. The samples were filtered through a 0.2 μm membrane to remove insoluble impurities. For spiking experiments, the river water was spiked with 20 nM and 200 nM of Co^{2+}, respectively. The pond water was spiked with 30 nM and 300 nM of Co^{2+}, respectively. Given that A_{535}/A_{690} falls outside the linear detection range, sample dilution by adding distilled water is needed. The spiked samples were detected using the proposed procedures, and the recoveries and relative standard deviations (RSDs) were calculated.

3. Results and discussion

3.1 Feasibility of Co^{2+} detection using CGNs

CGNs have a specific morphology with 8 tips and 6 concave surfaces, which were applied as a novel sensitive probe for Co^{2+} detection in this study. The feasibility was verified by recording the photo and UV-vis spectra of a CGN solution (Fig. 1A). CGNs were synthesized by following a mature method with the use of AA and H_2O_2 as co-reducing agents.[17] The as-obtained CGNs have two typical adsorption peaks at 690 nm and 535 nm, corresponding to their longitudinal and transverse localized surface plasmon, respectively, similar to gold nanostars.[20] The color of the CGN solution is blue. A small amount of CTAB (0.6 mM) was added to the solution in order to stabilize CGNs and prevent their aggregation. With the addition of 0.2 mM SCN^-, 0.02 mM HCO_3^-, and 370 mM H_2O_2, the UV-vis curve of CGNs exhibited no change. However, in the presence of 400 nM Co^{2+}, only one strong peak at 535 nm was observed and the solution color obviously changed to red. Here, H_2O_2 was in excess, but it did not etch CGNs because the oxidizing capacity of H_2O_2 is pH dependent and the solution pH make it not a strong oxidant. Thus, it is Co^{2+} that triggers the etching of CGNs, causing a variation in their solution color and LSPR, which was employed for constructing an assay for Co^{2+} detection.

The TEM images of CGNs before and after being etched in the presence of Co^{2+} are shown in Fig. 2. The as-synthesized CGNs have a well-defined concave structure with six concave faces and eight sharp corners (Fig. 2A), exhibiting good dispersion, similar to that previously reported.[17,24] The size of CGNs (outer diameter) is 90.2 ± 3.5 nm. In the presence of 100 nM Co^{2+}, CGNs underwent pronounced morphological evolution. Their eight tips were notably shortened, and the overall concavity of the particles drastically decreased. While some nanoparticles still retained slight surface concavity, a small fraction transformed into rounded cubic structures (Fig. 2B). This is attributed to the higher reaction activity of the eight corners on CGNs, which preferentially undergo dissolution, leading to tip blunting and reduction in concavity. The size of CGNs was reduced to 74.2 ± 2.9 nm. With a higher Co^{2+} concentration (Fig. 2C), CGNs were etched into spherical gold nanoparticles. Their corners and tips disappeared, with the size of CGNs reduced to 48.1 ± 1.8 nm. Also, their surfaces were flattened. This etching behavior is attributed to the preferential oxidation of Au atoms at the high-activity corners and edges.[16] It is reasonable that the specific morphology of CGNs results in high-index faces, *e.g.*, {730} and {720}, and the Au atoms at the edge or corner of CGNs have less than 12 neighbors (Au atom in a face-centered cubic structure has 12 neighbors), which have high chemical activity and are readily etched. This is the key reason why we used CGNs as a probe to enhance the sensitivity for Co^{2+} detection.

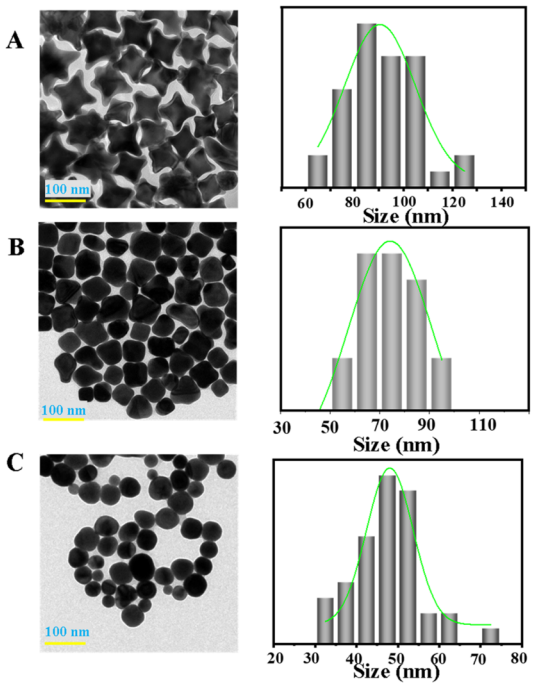

Fig. 2 TEM images (left) and particle diameter distributions (right) of CGNs before (A) and after being etched in the presence of 100 nM Co^{2+} (B) and 400 nM Co^{2+} (C). The concentrations of KSCN, $NaHCO_3$, and H_2O_2 for etching are 2 mM, 2.5 mM, and 370 mM, respectively.

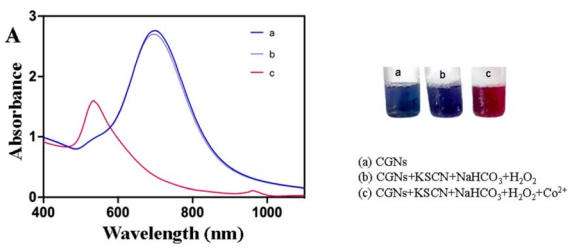

Fig. 1 Detection of Co^{2+} using CGNs based on Co^{2+} induced Fenton-like reactions. (A) UV-vis spectra (left) and photos (right) of CGNs (a), CGNs + KSCN + $NaHCO_3$ + H_2O_2 (b) and CGNs + KSCN + $NaHCO_3$ + H_2O_2 + Co^{2+} (c). The concentrations of KSCN, $NaHCO_3$, H_2O_2 and Co^{2+} are 2 mM, 2.5 mM, 370 mM, and 400 nM, respectively.

Fenton-like reactions induced by Co^{2+} have already been reported in previous studies.[23,25,26] In detail, in the presence of H_2O_2 under alkaline conditions, Co^{2+} catalyzes the decomposition of H_2O_2 to generate $^{\bullet}OH$ and $HO_2^{\bullet}$ radicals, which further convert to superoxide radicals $O_2^{\bullet-}$.[26] The resulting abundant

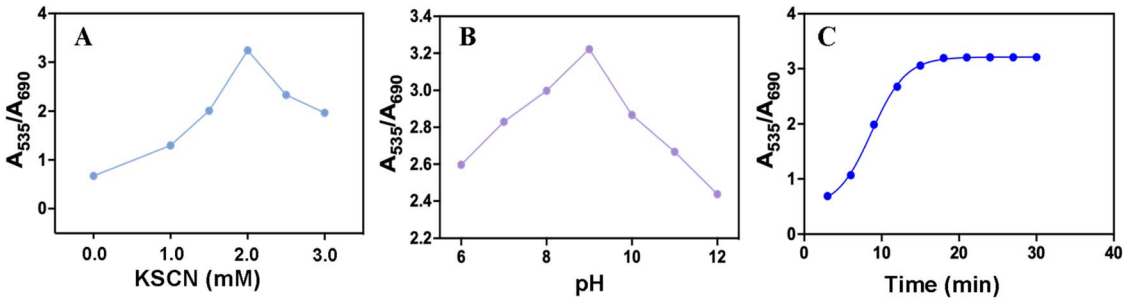

Fig. 3 Effect of KSCN concentration (A), solution pH (B) and incubation time (C) on Co^{2+} detection. The conditions are: (A) 2.5 mM $NaHCO_3$, 400 nM Co^{2+}, 370 mM H_2O_2, and 20 min; (B) 2.0 mM SCN^-, 400 nM Co^{2+}, 370 mM H_2O_2, and 20 min; and (C) 2 mM SCN^-, pH 9.0, 400 nM Co^{2+}, and 370 mM H_2O_2.

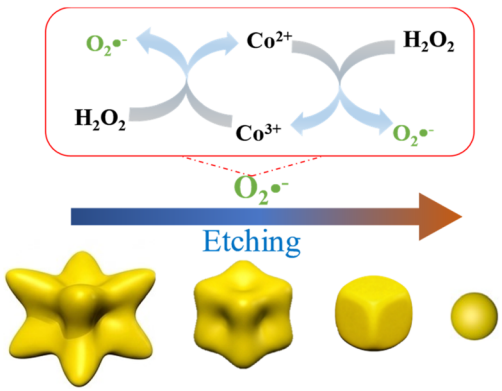

Scheme 1 Mechanism for Co^{2+} sensing by the Fenton-like reaction-mediated etching of concave gold nanocubes to spherical gold nanoparticles.

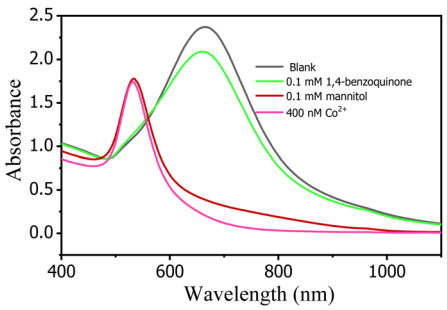

Fig. 4 UV-vis spectra of CGN solutions containing different chemicals after incubation at 80 °C for 18 min. The blank solution contained 2 mM KSCN and 370 mM H_2O_2 at pH 9.0.

$O_2^{\bullet-}$ oxidizes Au^0 on the surface of CGNs to Au^+, which forms a stable complex with SCN^- ($Au(SCN)_2^-$) with a spherical morphology. Although $OH^\bullet$ demonstrates strong oxidizing capacity, it does not take part in the etching directly and is probably transformed into $HO_2^\bullet$ quickly in the system[27] because the presence of its quencher, mannitol, did not stop the reaction (Fig. 3). In contrast, the addition of a quencher for $O_2^{\bullet-}$, 1,4-benzoquinone, halted the etching efficiently.[28] Due to the high stability of the $[Au(SCN)_2]^-$ complex ($\log \beta_2 \approx 26$), SCN^- facilitates a continuous and efficient etching process that improves the detection sensitivity.[29] Finally, this process leads to the etching of CGNs into spherical gold nanoparticles, resulting in a blue shift in their LSPR and an obvious color change. The key reactions are as follows:

$$Co^{2+} + H_2O_2 \rightarrow Co^{3+} + {}^\bullet OH + OH^- \quad (1)$$

$$^\bullet OH + H_2O_2 \rightarrow H_2O + HO_2^{\bullet-} \quad (2)$$

$$H_2O_2 + Co^{3+} \rightarrow HO_2^\bullet + H^+ + Co^{2+} \quad (3)$$

$$HO_2^\bullet \rightarrow O_2^{\bullet-} + H^+ \quad (4)$$

$$Au + O_2^{\bullet-} + 2SCN^- + 2H_2O \rightarrow Au(SCN)_2^- + H_2O_2 + 2OH^- \quad (5)$$

Therefore, the mechanism for Co^{2+} detection using CGNs is that Co^{2+} catalyzes the decomposition of H_2O_2 to yield abundant $O_2^{\bullet-}$, which etches CGNs and causes a transformation in their shape as well as their corresponding LSPR properties (Scheme 1).

3.2 Optimization of reaction parameters

To ensure the reliable detection of Co^{2+}, the influence of different parameters, including SCN^- concentration, pH, and reaction time, was systematically investigated (Fig. 4). SCN^- plays a dual role in the etching system: it acts as a complexing agent for Au^+ and as a mediator that enhances the anisotropic etching of CGNs.[29] At low concentrations (<1.0 mM), only a weak LSPR shift and negligible color change were observed, indicating the insufficient etching of CGNs (Fig. 4A). Increasing the concentration of KSCN to 2.0 mM resulted in a pronounced variation in A_{535}/A_{690} and an intense visual color transition, demonstrating efficient chemical etching. In contrast, a further increase in KSCN concentration to 3.0 mM did not cause excessive etching. This is because excess SCN^- would be adsorbed on the positively charged CGNs, disrupting the stability of the nanoparticles and leading to their partial aggregation.[30] Thus, 2.0 mM of SCN^- was chosen as the optimal concentration.

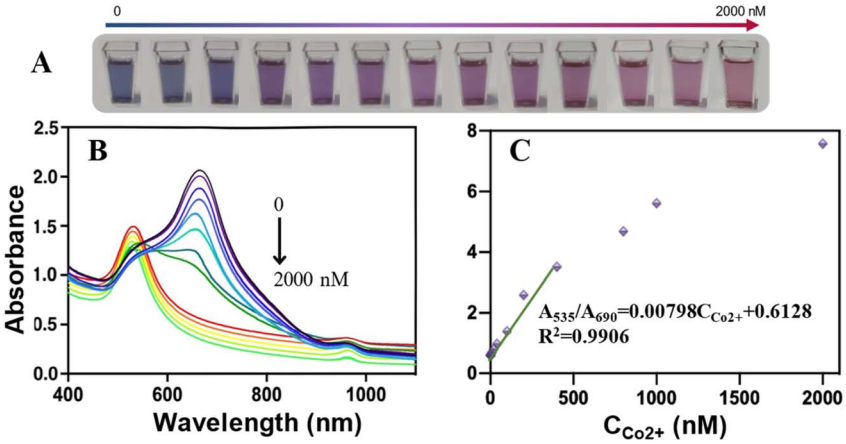

Fig. 5 Photographs (A), UV-vis spectra (B) and A_{535}/A_{690} (C) of CGNs after incubation with different concentrations of Co^{2+} at 80 °C for 18 min at pH 9.0. The concentration of H_2O_2 and KSCN is 370 mM and 2 mM, respectively.

Table 1 Comparison of the colorimetric methods for Co^{2+} detection

Materials	Working range (nM)	LOD (nM)	References
Ag–Au bimetallic nanoparticles	0–60	20	39
Gold nanoparticles	60–2200	113	40
Silver nanoparticles	1700–20000	680	41
Gold nanoparticle	50–1600	3.5	42
Core-satellite gold nanoparticle	100–10000	10	35
CGNs	0.5–100	0.3	This work

The pH of the reaction medium is another critical factor, as it governs the catalytic activity of Co^{2+} and the stability of radicals. At pH < 7, etching proceeded very slowly, with a minimal optical response (Fig. 4B). The reason for this is that pH regulates the generation, transformation and quenching of free radicals.[31] Acidic conditions lead to the protonation of the radicals and reduce the lifetime of radicals such as $^{\bullet}OH$, $O_2^{\bullet-}$, and $HO_2^{\bullet}$ from the microsecond scale to the nanosecond scale, hindering the etching of CGNs.[32] Increasing pH would enhance the etching effect and result in larger LSPR shifts and a variation in A_{535}/A_{690}. At pH 9.0, the system achieved the maximum sensitivity and a stable performance, whereas excessively high alkalinity (pH > 10) led to smaller changes. The reason for this is that the nonspecific decomposition of H_2O_2 increases markedly with an increasing solution pH over 9.5–12.[33] Higher pH would reduce the stability of the nanoparticle suspension and the catalytic activity of Co^{2+} in generating $O_2^{\bullet-}$ radicals because of the formation of $Co(OH)_2$.[34] Therefore, pH 9.0 was selected as the optimal condition. Under this condition, the $NaHCO_3$ concentration is 2.5 mM.

The reaction kinetics were evaluated by monitoring the variation in A_{535}/A_{690} at intervals of 3 min (Fig. 4C). During the first 15 min, the A_{535}/A_{690} changes were pronounced, with an upward trend. However, an extension of the incubation time beyond 18 min did not produce further changes, suggesting that the etching process reached equilibrium. Consequently, the reaction time of 18 min was optimal. Collectively, these results established the optimal sensing conditions as 2.0 mM KSCN at pH 9.0 with an incubation period of 18 min. Under these conditions, the Fenton-like reaction-induced etching was sufficiently rapid, reproducible, and sensitive for reliable Co^{2+} detection.

3.3 Sensitivity and selectivity

The analytical performance of the CGN probe for sensing Co^{2+} was systematically evaluated under the optimized conditions. The UV-vis spectra with the introduction of increasing Co^{2+} concentration (0–2000 nM) are shown in Fig. 5. Obviously, with an increasing Co^{2+} concentration, an obvious color change from blue to red was observed and a gradual increase in A_{535}/A_{690} was evident, accompanied by a gradual blueshift in the longitudinal LSPR peak position (Fig. 5A and B). A good linear relationship between A_{535}/A_{690} and Co^{2+} concentration was obtained over the range of 0.5–400 nM, and the regression equation is $A_{535}/A_{690} = 0.00798C + 0.6128$ (Fig. 5C). The correlation coefficient is $R^2 = 0.9906$, highlighting the excellent linearity and reproducibility of the assay. The LOD was calculated as 3σ/slope, which is 0.3 nM, surpassing the sensitivity of most conventional colorimetric sensors. For example, based on disrupting the structures of core-satellite gold nanoparticles, Co^{2+} was determined with an LOD of 10 nM.[35] Because Co^{2+} can directly induce the aggregation of citrate-stabilized gold nanoparticles, it could be detected over the range of 0.1 μM to 15 μM, with an LOD of 1 nM.[36] Furthermore, the visual color change from blue to red was clearly discernible to the naked eye at concentrations above

30 nM, confirming the potential of this system for rapid and on-site detection without specialized instrumentation. This high sensitivity is attributed to three key reasons. (i) The detection was based on the catalysis of Co^{2+} to form radicals and thus the etching of Au^0 could be enhanced by tens of thousands of times. (ii) CGNs are an excellent probe for Co^{2+} detection because of their specific morphology, where their tips and corners offer a large number of active sites for Au^0 to be etched.[20] (iii) The morphology-dependent LSPR of CGNs underwent strong variation after their etching. Compared to other classical colorimetric sensors, the present method exhibits overwhelming advantages in terms of the high sensitivity and good stability of the probe (Table 1).[18] These results demonstrate that the proposed assay is a promising platform for trace Co^{2+} detection. With the rapid advancement of artificial intelligence, tremendous opportunities may emerge for this sensor including the rational design and tuning of CGNs, intelligent and instrument-free data reading *via* smartphone imaging, and automatic signal denoising and interference correction for improved detection accuracy.[37,38]

It should be pointed out that the synthesis of CGNs may vary from batch to batch, even when performed by the same operator. Also, the LSPR of CGNs could undergo slight changes after long-term storage. To overcome these shortcomings, a working curve should be established prior to each detection. Although the slope may differ slightly, the accuracy of Co^{2+} detection remains satisfactory using this strategy.

The selectivity of the sensing platform is critical for its real applications and thus was investigated in the presence of a variety of potentially interfering metal ions, including Mn^{2+}, Hg^{2+}, Cu^{2+}, Ca^{2+}, Pb^{2+}, Cd^{2+}, Zn^{2+}, Sn^{2+}, Li^{+}, Na^{+}, Ni^{2+}, and Fe^{3+} (Fig. 6). Their concentrations were 1000 nM, while the concentration of Co^{2+} was 100 nM. Apparently, for these ions, negligible changes in solution color and absorbance were observed, even at 10-fold higher concentrations than that of Co^{2+}. In contrast, Co^{2+} induced a pronounced decrease in the intensity at the longitudinal LSPR and a distinct color variation from blue to red due to the etching-induced morphological transformation of CGNs to spherical shapes. Notably, the Fe^{3+}–H_2O_2 system is a classic Fenton-like oxidation process that generates highly oxidative $^{\cdot}OH$ as the main reactive oxygen species. However, this system only operates efficiently under acidic conditions (pH 2.0–4.0). In contrast, our system is maintained at pH 9.0, which significantly suppresses the Fenton-like reaction and the formation of $^{\cdot}OH$. Furthermore, the addition of SCN^{-} promotes the formation of stable complexes with Fe^{3+}, reducing the concentration of free Fe^{3+} and further minimizing oxidative interference caused by iron ions. Thus, this new platform demonstrates excellent specificity toward Co^{2+}. Its superior selectivity can be attributed to the unique catalytic activity of Co^{2+} in the Fenton-like system.[23] Specifically, Co^{2+} efficiently catalyzes the decomposition of H_2O_2 in the presence of bicarbonate, generating $O_2^{\cdot -}$ radicals that selectively etch CGNs. Other tested cations lack this catalytic activity, while other ions do not have this ability.

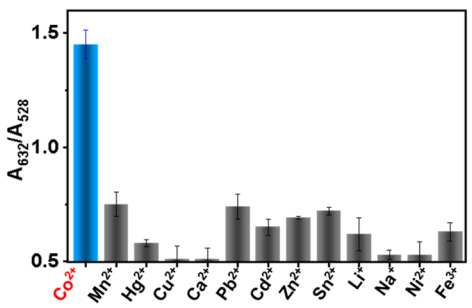

Fig. 6 Response of CGNs to other metal ions including Mn^{2+}, Hg^{2+}, Cu^{2+}, Ca^{2+}, Pb^{2+}, Cd^{2+}, Zn^{2+}, Sn^{2+}, Li^{+}, and Na^{+} with their concentration at 1000 nM. 100 nM of Co^{2+} is the positive control.

Table 2 Cobalt ion detection in water samples ($n = 3$)

Sample	Added (nM)	Detected (nM)	Recovery (%)	RSD (%)
River water	0	Not detected	—	—
	20	20.9	104.5	4.9
	200	203.3	101.7	3.7
Pond water	0	Not detected	—	—
	30	31.2	104.0	4.3
	300	295.8	98.1	3.9

3.4 Real sample analysis

To further evaluate its practical applicability, the method was verified for the detection of water samples collected from the Xiang River and a pond in a hospital (Table 2). The samples were treated first by filtering them through a 0.22 μm membrane to remove large suspended particulates and then directly analyzed. The two water samples contained a Co^{2+} content below the LOD. Then, the samples were also spiked and tested. It was found that the recoveries range from 98.1% to 104.5%, with RSDs below 5.0% ($n = 3$), confirming both the accuracy and precision of our method in real water samples. Importantly, the distinct colorimetric response could be distinguished by naked eyes in the spiked samples, highlighting the potential of this platform for rapid, on-site detection without the need for sophisticated instrumentation. Compared with conventional techniques such as AAS, ICP-AES, and ICP-MS, the developed method offers the advantages of simplicity, low cost, instrument-free operation, and portability, while still achieving satisfactory accuracy for trace-level detection. These results strongly demonstrate that the new sensing platform using CGNS based on Fenton-like reactions is highly valuable for environmental monitoring and food-safety analysis.

4. Conclusions

In summary, we developed a novel colorimetric sensing platform for the highly sensitive and selective detection of Co^{2+} using CGNs as a novel probe based on Fenton-like reactions. The shape-dependent optical properties of CGNs and the highly reactive sites due to their abundant high-index facets are responsible for their high sensitivity. In the presence of Co^{2+},

bicarbonate, H_2O_2, and $O_2^{\bullet-}$ were generated *via* a catalytic reaction, which etched CGNs, leading to morphological changes to spherical gold nanoparticles. Thus, obvious LSPR optical properties and visually observable color changes were observed. Under these conditions, the plot of A_{535}/A_{690} *vs.* Co^{2+} concentration for the sensor exhibited its excellent analytical performance, including a linear response over 0.5–400 nM ($R^2 = 0.9906$), with an LOD of 0.3 nM and a naked-eye detection threshold of ~30 nM. This sensor also displayed remarkable selectivity, with negligible interference from common coexisting metal ions because these ions cannot induce Fenton-like reactions. Its application for the analysis of real drinking water samples yielded recoveries of 98.1–104.5% with RSDs below 5.0%, confirming its accuracy, reliability, and practicality. Compared with conventional analytical methods, the proposed assay offers distinct advantages in simplicity and cost-effectiveness, making it highly attractive for on-site monitoring. This method shows promise for applications in food safety testing, biomedical diagnostics, and rapid screening of heavy metal contamination. Furthermore, morphology-dependent etching of anisotropic nanostructures provides a versatile platform for the detection of other hazardous ions or biomolecules through the rational design of the reaction conditions.

Conflicts of interest

There are no conflicts to declare.

Data availability

All data supporting this study, including UV-Vis spectra, absorbance measurements, photographs of solutions, and TEM images, are contained within the main text of the article.

Acknowledgements

This work was supported by funding from the Xiangya Hospital of Central South University Program on Postgraduate Medical Education Research and 2024–2025 Central South University General Program on Teaching Reform of Academic Degree and Graduate Education.

References

1 G. Genchi, G. Lauria, A. Catalano, A. Carocci and M. S. Sinicropi, *Biology*, 2023, **12**, 1335.
2 M. R. Islam, S. Akash, M. H. Jony, M. N. Alam, F. T. Nowrin, M. M. Rahman, A. Rauf and M. Thiruvengadam, *Mol. Cell. Biochem.*, 2023, **478**, 2141–2171.
3 L. O. Simonsen, H. Harbak and P. Bennekou, *Sci. Total Environ.*, 2012, **432**, 210–215.
4 M. H. Uddin and M. Rumman, in *Metal Toxicology Handbook*, CRC Press, 2020, pp. 273–285.
5 N. M. P. Coelho, F. Bernardo, A. S. Rodrigues and P. Garcia, *Sci. Total Environ.*, 2025, **993**, 180018.
6 L. Leyssens, B. Vinck, C. Van Der Straeten, F. Wuyts and L. Maes, *Toxicology*, 2017, **387**, 43–56.
7 D. J. Paustenbach, B. E. Tvermoes, K. M. Unice, B. L. Finley and B. D. Kerger, *Crit. Rev. Toxicol.*, 2013, **43**, 316–362.
8 M. Ghaedi, F. Ahmadi and A. Shokrollahi, *J. Hazard. Mater.*, 2007, **142**, 272–278.
9 E. P. Galay, R. V. Dorogin and A. Z. Temerdashev, *Heliyon*, 2021, **7**, e06046.
10 D. Singhal, A. K. Singh and A. Upadhyay, *Mater. Sci. Eng., C*, 2014, **45**, 216–224.
11 E. M. Sullam, K. M. Adam, J. Liu, H. Chen and J. Xiao, *Chin. Chem. Lett.*, 2024, **35**, 108476.
12 H. Duman, E. Akdaşçi, F. Eker, M. Bechelany and S. Karav, *Nanomaterials*, 2024, **14**, 1805.
13 H. Chen, S. Cai, J. Luo, X. Liu, L. Ou, Q. Zhang, B. Liedberg and Y. Wang, *TrAC, Trends Anal. Chem.*, 2024, **173**, 117654.
14 N. T. T. Phuong, H. A. Nguyen, T. N. D. Trinh and K. T. L. Trinh, *Anal. Methods*, 2025, **17**, 4496–4509.
15 T. Xu and Z. Geng, *Biosens. Bioelectron.*, 2021, **174**, 112850.
16 H. Luo, M. Ouyang, H. Li, S. Nie, D. Xu and T. Zhao, *Inorg. Chem.*, 2024, **63**, 13110–13116.
17 R. Zhou, H. Luo, C. Peng, X. Guo, T. Zhao, Y. Du, D. Xu and Q. Lin, *Chem. Eng. J.*, 2023, **470**, 144044.
18 E. T. Athira and J. Satija, *Analyst*, 2023, **148**, 6188–6200.
19 S. Yadav and J. Satija, *Nanoscale Adv.*, 2022, **4**, 3928–3939.
20 S. Wang, X. Huang, Q. An, R. Zhou, W. Xu, D. Xu, Q. Lin and X. Cao, *Anal. Chim. Acta*, 2021, **1160**, 338380.
21 Y.-Y. Chen, H.-T. Chang, Y.-C. Shiang, Y.-L. Hung, C.-K. Chiang and C.-C. Huang, *Anal. Chem.*, 2009, **81**, 9433–9439.
22 S. Wang, J. Sun, J. Cao, K. Lu and D. Xu, *J. Chin. Chem. Soc.*, 2024, **71**, 820–828.
23 Z. Zhang, Z. Chen, D. Pan and L. Chen, *Langmuir*, 2015, **31**, 643–650.
24 J. Zhang, M. R. Langille, M. L. Personick, K. Zhang, S. Li and C. A. Mirkin, *J. Am. Chem. Soc.*, 2010, **132**, 14012–14014.
25 S.-X. Liang, L.-X. Zhao, B.-T. Zhang and J.-M. Lin, *J. Phys. Chem. A*, 2008, **112**, 618–623.
26 X. Li, Z. Xiong, X. Ruan, D. Xia, Q. Zeng and A. Xu, *Appl. Catal., A*, 2012, **411**, 24–30.
27 G. J. Magovern Jr, S. F. Bolling, A. S. Casale, B. H. Bulkley and T. J. Gardner, *Circulation*, 1984, **70**, I91–I95.
28 M. Zhu, J. Lu, Y. Hu, Y. Liu, S. Hu and C. Zhu, *Environ. Sci. Pollut. Res.*, 2020, **27**, 31289–31299.
29 A. Y. S. Zeebaree, O. I. H. Zebari, S. Y. S. Zeebaree, R. D. Thanoon and Y. N. Yaseen, *Arabian J. Chem.*, 2023, **16**, 105297.
30 G. Cabello, X. J. Chen, R. Panneerselvam and Z. Q. Tian, *J. Raman Spectrosc.*, 2016, **47**, 1207–1212.
31 J. Liang, K. Chen, X. Duan, L. Zhao, H. Qiu, X. Xu and X. Cao, *Water Res.*, 2022, **224**, 119113.
32 B. H. Bielski and A. O. Allen, *J. Phys. Chem.*, 1977, **81**, 1048–1050.
33 A. Rastinfard, B. Dalisson and J. Barralet, *Acta Biomater.*, 2022, **145**, 390–402.
34 M. Adeel, V. Canzonieri, S. Daniele, F. Rizzolio and M. M. Rahman, *J. Ind. Eng. Chem.*, 2021, **103**, 165–174.

35 F. Mazur, L. Liu, H. Li, J. Huang and R. Chandrawati, *Sens. Actuators, B*, 2018, **268**, 182–187.
36 R. Raghav and S. Srivastava, *Sens. Lett.*, 2015, **13**, 254–258.
37 P. Jiang, Y. Dai, Y. Hou, J. Stein, S. S. Lin, C. Zhou, Y. Hou, R. Zhu, K.-B. Lee and L. Yang, *BMEMat*, 2025, **3**, e70004.
38 L. Qiao, Y. Shen, S. Zhang, M. Wang, G. Lv, Q. Dou and C. Li, *BMEMat*, 2023, **1**, e12011.
39 D. Xu, H. Chen, Q. Lin, Z. Li, T. Yang and Z. Yuan, *RSC Adv.*, 2017, **7**, 16295–16301.
40 G. Ravi, N. Divesh, R. Srivastava and P. Gupta, Paul and Debdeep, *Sens. Actuators, B*, 2014, **191**, 757–764.
41 M. Zafer, C. S. Keskin and A. Zdemir, *Spectrochim. Acta, Part A*, 2020, **239**, 118487.
42 C. Karami and M. A. Taher, *Plasmonics*, 2018, **13**, 1315–1323.